IET Optoelectronics

Research Article

IET Journals
The Institution of Engineering and Technology

Highly steerable microwave beamforming system near Ku band based on the application of linearly CFBG

ISSN 1751-8768
Received on 30th May 2019
Revised 15th October 2019
Accepted on 25th November 2019
E-First on 4th February 2020
doi: 10.1049/iet-opt.2019.0073
www.ietdl.org

Sanjeev Kumar Raghuwanshi[1], Nimish Kumar Srivastava[1] ✉, Mandeep Singh[2]

[1]Department of Electronics Engineering, Indian Institute of Technology (Indian School of Mines), Dhanbad 826 004, Jharkhand, India
[2]Department of Electronics and Communication Engineering, National Institute of Technology Karnataka, Surathkal 575 025, Karnataka, India
✉ *E-mail: nimish11@ece.ism.ac.in*

Abstract: In this study, the authors present theoretical and experimental results of wideband beamforming networks steered by a single linear chirped fibre Bragg grating (CFBG). The standard single-sideband modulation technique is followed to validate the wideband (at 18 GHz) operation of the proposed system. CFBG has been fabricated by phase mask technology for the desired specification to be compatible with the antenna array. To the authors knowledge, the effect of dispersion slope feature of fabricated FBG on the performance of beam-steering capability of the antenna is reported for the first time in this study. Theoretically preceded by experimental testing, it was found that the scanning angle increased with the rise in the number of antenna elements and the frequency of modulating microwave signal.

1 Introduction

Microwave beam steering by using photonic technique has been under intensive research over the last three decades [1–5]. Modern radar and satellite require the use of a highly beam-steerable phase array antenna (PAA). There are several benefits of optical fibre to be used in microwave beamforming networks such as low weight, no electromagnetic interference, high bandwidth, data security, signal reliability, and advanced manufacturing techniques to name but a few [6]. Fibre Bragg grating (FBG) was used as an active optical tool for realising a real-time-delay line. Earlier discrete FBG-based [7, 8] true time-delay (TTD) line was proposed, which would eventually end up with chirped FBG (CFBG) [9] for the implementation of a very flexible beam-steering system. The TTD module, consisting of a pair of CFBG, is typically used to maintain the beam orientation continuously in the desired direction at variable microwave frequencies during the movable state. It is a matter of fact that the radiation pattern of the antenna array and its beam-pointing directions remain invariant for the change in the frequency of microwave signal. It is also known that the beam-pointing direction can be continuously steered by changing the optical wavelength. The CFBG has been proven to be an excellent technique for the beamforming network. The need for long-length chirp grating may be resolved by small-length multi-channel CFBG. Discrete FBG-based TTD can achieve discrete beam-pointing angles and is only suitable for low microwave frequency but CFBG enables continuous beam control and can operate at a very high frequency. The optical system for steering the microwave waveform also offers the benefit of simultaneous beam multiplexing capabilities for multipoint beam directions. Several configurations based on FBG delay lines have been proposed in the past [10–15]. Nevertheless, the use of a single CFBG-based TTD provides much more flexibility and cost-effective implementation of a wideband beamforming system. It has been shown that even a single FBG chirped is capable of directing the microwave beam at very high frequency extended beyond the Ku band.

The beam can be more concentrated by increasing the number of antenna arrays [16–18]. The beam can also be operated in two different directions by integrating a two-dimensional (2D) antenna array. The main advantage provided by photonic-based TTD line techniques is the wideband squint-free beam steering along with the advantages offered by optical fibre technology. Highly CFBG [19–21] has provided extremely promising applications for high-speed photonic PAA systems [22–24]. To the best of our knowledge, the beam-steering capability provided by featured CFBG has not yet exploded. It has been shown that instead of the linear phase shift (or time delay) introduced by the featured FBG, the linear chirp FBG provides a slightly non-linear symmetric phase shift with a large dispersion slope and a two-fold increase in the number of antenna elements driven by the linear chirp FBG. In this paper, study has been conducted on the photonic beam-steering capability of the antenna array versus CFBG design parameters such as grating length, chirp factor, index contrast, chirp profile etc. Change in the design parameter of the CFBG keeps changing the time-delay response of the TTD unit, which ultimately results in a change in the direction of beam steering. Results have been shown for $\Omega = 3, 6, 13, 18$ GHz, i.e. S–Ku-band frequency bands. It is a matter of fact that 1000 ps time delay can be easily steered to 16 antenna elements at a microwave frequency of 18 GHz. Therefore, the proposed design is capable of steering at least 16 antenna elements at the Ku band.

Table 1 indicates the maximum spacing between each element of PAA required relative to the modulating microwave frequency. In short, Table 2 presents the comparison between the photonic approaches of wideband versus conventional beam steering. This paper is structured in the following ways. Mathematical analysis of single-sideband (SSB) modulation technique is covered in Section 2. This section showcases the delay response of CFBG when lightwave is intensity modulated by different microwave frequencies such as 3, 6, 13, and 18 GHz. Section 3 demonstrates the experimental response of a CFBG of 5 nm spectral width, when an optical carrier is being SSB modulated. This section also shows the computed radiation patterns of 4, 8, 12, and 16 elements antenna, which was driven by a time-delayed radio-frequency (RF) signal. Finally, Section 4 presents the concluding remarks of this paper.

Table 1 Antenna spacing for different microwave frequency

Sl. no.	Operating frequency, GHz	Antenna spacing, mm
1	3	50
2	6	25
3	13	11.53
4	18	8.33

Table 2 Comparison of wideband beam steering with conventional beam-steering techniques

Sl. no.	Time-delay module	Scheme	Bandwidth, GHz	Scanning method	Delay range
1	Silicon waveguide	binary 2 × 2 switches, MZM	8–12	Discrete	≃2.5 ns
2	Dispersive fibre-prism	Tunable laser source (TLS) with Multiplexer	4–8	Continuous	≃28 ps
3	Dispersive photonic crystal fibre	TLS four fibre channels, MZM	8–12	Continuous	±31 ps
4	Dispersion compensation fibre	TLS eight channels, MZM	8–12	Continuous	±43.3 ps
5	Fibre-prism and fibre-optic delay lines	2D, 2 × 2 switches	1	Switchable	±200 ps
6	Linearly CFBG[a]	TLS, MZM wavelength-dependent grating	12	Continuous	±1500 ps

[a]Proposed scheme.

2 Proposed experimental setup and its operating principle

In this paper, we present the experimental results of the featured CFBG developed in our collaborative laboratory. The following novelty was claimed in this paper in comparison with the existing study found in the literature: (i) CFBGs have been fabricated using a phase mask technique in our collaborative laboratory with the requisite specification such as high chirp rate, centre wavelength, refractive index contrast, and apodisation parameter to mention a few, (ii) CFBG characteristics have been analysed using optical spectrum analyser (OSA) and multiple channel optical interrogator (HBM:FS22 DI), and (iii) the antenna array has been fabricated with the required specification at Empower Technology Pvt. Ltd. The effects of dispersion slope and ripple factor due to chirp grating reflectivity were analysed experimentally.

2.1 Working principle

It is known that the CFBG generates almost linear phase delay between the modulating microwave frequencies, which can be continuously changed by adjusting the output wavelength of the tunable laser source. However, a large number of antenna arrays are required to achieve a sharp beam-pointing direction. Also, if it is desirable to steer the beam in multiple directions in 2D space, a 2D antenna array with sub-array partitioning capability is required, resulting in a mathematically complex analysis. In this paper, an SSB modulation technique has been opted to steer the beam so that the constraint of the high-frequency microwave waveform can be nullified. The experimental measurement of the 5 nm chirped grating response is observed, while the lightwave is intensity modulated by RF wave using dual-drive Mach–Zehnder modulator (MZM), which generates an SSB modulated optical signal. FBG reflectivity and time-delay responses are measured within the grating response range at multiple RF frequencies.

To show the upper hand of SSB modulation over DSB modulation based on performance, we are first rigorously deriving mathematical expressions by keeping in mind a conventional DSB technique. An optical carrier having frequency ω is intensity modulated by a microwave signal of frequency Ω. Suppose the lightwave is being modulated by DSB scheme, which is further reflected by a CFBG having reflectivity $R(\omega) = R_0(\omega)\,\mathrm{e}^{\mathrm{j}\phi(\omega)}$. Now, the output electric field from CFBG is the sum of following terms $R(\omega) = R_0(\omega)\,\mathrm{e}^{\mathrm{j}\phi(\omega)}$, $R_0(\omega+\Omega) = R_0(\omega)\,\mathrm{e}^{\mathrm{j}\phi(\omega+\Omega)t}$, and $R_0(\omega-\Omega) = R_0(\omega)\,\mathrm{e}^{\mathrm{j}\phi(\omega-\Omega)t}$. The modulated signal has double-sideband frequency components given by

$$x(t) = A_1\mathrm{e}^{\mathrm{j}\omega t} + A_2\mathrm{e}^{\mathrm{j}(\omega-\Omega)t} + A_2\mathrm{e}^{\mathrm{j}(\omega+\Omega)t} \tag{1}$$

The above-modulated signal is reflected by a fibre grating of reflectivity $\boldsymbol{R(\omega)} = R(\omega)\mathrm{e}^{\mathrm{j}\phi(\omega)}$, which gives the following field at the input of PD:

$$y(t) = \boldsymbol{R(\omega)}\mathrm{e}^{\mathrm{j}\omega t} + \boldsymbol{R(\omega-\Omega)}\mathrm{e}^{\mathrm{j}(\omega-\Omega)t} + \boldsymbol{R(\omega+\Omega)}\mathrm{e}^{\mathrm{j}(\omega+\Omega)t} \tag{2}$$

$$\begin{aligned} y(t) &= (R(\omega)\mathrm{e}^{\mathrm{j}\phi(\omega)} + R(\omega-\Omega)\mathrm{e}^{\mathrm{j}\phi(\omega-\Omega)}\mathrm{e}^{-\mathrm{j}\Omega t} \\ &\quad + R(\omega+\Omega)\,\mathrm{e}^{\mathrm{j}\phi(\omega+\Omega)}\,\mathrm{e}^{\mathrm{j}\Omega t})\,\mathrm{e}^{\mathrm{j}\omega t} \\ y^*(t) &= (R(\omega)\mathrm{e}^{-\mathrm{j}\phi(\omega)} + R(\omega-\Omega)\mathrm{e}^{-\mathrm{j}\phi(\omega-\Omega)}\,\mathrm{e}^{\mathrm{j}\Omega t} \\ &\quad + R(\omega+\Omega)\mathrm{e}^{-\mathrm{j}\phi(\omega+\Omega)}\,\mathrm{e}^{-\mathrm{j}\Omega t})\,\mathrm{e}^{-\mathrm{j}\omega t} \end{aligned} \tag{3}$$

Electric field detected by PD is given by $E(t) \propto |y(t)|^2$

$$\begin{aligned} E(t) &= y(t)\,y^*(t) \\ &= (R(\omega)\mathrm{e}^{\mathrm{j}\phi(\omega)} + R(\omega-\Omega)\mathrm{e}^{\mathrm{j}\phi(\omega-\Omega)}\,\mathrm{e}^{-\mathrm{j}\Omega t} + R(\omega+\Omega)\cdot \\ &\quad \mathrm{e}^{\mathrm{j}\phi(\omega+\Omega)}\,\mathrm{e}^{\mathrm{j}\Omega t})\,(R(\omega)\mathrm{e}^{-\mathrm{j}\phi(\omega)} + R(\omega-\Omega)\mathrm{e}^{-\mathrm{j}\phi(\omega-\Omega)}\cdot \\ &\quad \mathrm{e}^{\mathrm{j}\Omega t} + R(\omega+\Omega)\mathrm{e}^{-\mathrm{j}\phi(\omega+\Omega)}\,\mathrm{e}^{-\mathrm{j}\Omega t}) \\ &= R^2(\omega) + R^2(\omega-\Omega) + R^2(\omega+\Omega) + R(\omega)R(\omega-\Omega)\cdot \\ &\quad [\mathrm{e}^{\mathrm{j}(\phi(\omega)-\phi(\omega-\Omega))}\mathrm{e}^{\mathrm{j}\Omega t} + \mathrm{e}^{-\mathrm{j}(\phi(\omega)-\phi(\omega-\Omega))}\mathrm{e}^{-\mathrm{j}\Omega t}] + R(\omega) \\ &\quad R(\omega+\Omega)[\mathrm{e}^{\mathrm{j}(\phi(\omega+\Omega)-\phi(\omega))}\mathrm{e}^{\mathrm{j}\Omega t} + \mathrm{e}^{-\mathrm{j}(\phi(\omega+\Omega)-\phi(\omega))}\cdot \\ &\quad \mathrm{e}^{-\mathrm{j}\Omega t}] + R(\omega-\Omega)\,R(\omega+\Omega)[\mathrm{e}^{\mathrm{j}(\phi(\omega+\Omega)-\phi(\omega-\Omega))}\mathrm{e}^{\mathrm{j}2\Omega t} \\ &\quad + \mathrm{e}^{-\mathrm{j}(\phi(\omega+\Omega)-\phi(\omega-\Omega))}\mathrm{e}^{-\mathrm{j}2\Omega t}] \end{aligned} \tag{4}$$

Equation (4) gives the electric field detected by PD, which is passed through a narrow bandwidth bandpass filter. The bandpass filter will only allow the term containing Ω given by

$$\begin{aligned} E'(t) &= R(\omega)R(\omega-\Omega)\mathrm{e}^{\mathrm{j}(\phi(\omega)-\phi(\omega-\Omega))}\mathrm{e}^{\mathrm{j}\Omega t} + R(\omega)R(\omega+\Omega) \\ &\quad \cdot \mathrm{e}^{\mathrm{j}(\phi(\omega+\Omega)-\phi(\omega))}\mathrm{e}^{\mathrm{j}\Omega t} \\ &= R(\omega)(R(\omega-\Omega)\mathrm{e}^{\mathrm{j}(\phi(\omega)-\phi(\omega-\Omega))} + R(\omega+\Omega)\cdot \\ &\quad \mathrm{e}^{\mathrm{j}(\phi(\omega+\Omega)-\phi(\omega))})\mathrm{e}^{\mathrm{j}\Omega t} \end{aligned}$$

(see (5))

Above equation can be written in Euler form as

$$E'(t) = E(\omega,\,\Omega)\mathrm{e}^{\mathrm{j}\phi} \tag{6}$$

$$E(\omega,\,\Omega) = \sqrt{(\mathrm{Re}(E'(t)))^2 + (\mathrm{Im}(E'(t)))^2}$$

$$\begin{aligned} E(\omega,\,\Omega) &= R(\omega)((R(\omega-\Omega)\cos(\phi(\omega)-\phi(\omega-\Omega)) + R(\omega+\Omega)\,. \\ &\quad \cos(\phi(\omega+\Omega)-\phi(\omega)))^2 + (R(\omega-\Omega)\sin(\phi(\omega)-\phi \\ &\quad (\omega-\Omega)) + R(\omega+\Omega)\sin(\phi(\omega+\Omega)-\phi(\omega)))^2)^{1/2} \end{aligned} \tag{7a}$$

$$\phi = \Omega t + \tan^{-1}\frac{\mathrm{Im}(E'(t))}{\mathrm{Re}(E'(t))} \tag{7b}$$

After the conversion of optical to the electrical domain by 20 GHz photodetector (PD), the dependency of the electric field of output microwave signal on time can be expressed as

$$\begin{aligned} E'(t) &= R(\omega)(R(\omega-\Omega)\cos(\phi(\omega)-\phi(\omega-\Omega)) + R(\omega+\Omega) \\ &\quad \cos(\phi(\omega+\Omega)-\phi(\omega)) + \mathrm{j}(R(\omega-\Omega)\sin(\phi(\omega)-\phi(\omega-\Omega)) \\ &\quad + R(\omega+\Omega)\sin(\phi(\omega+\Omega)-\phi(\omega))))\mathrm{e}^{\mathrm{j}\Omega t} \end{aligned} \tag{5}$$

$$E(t) = E(\Omega, \omega)e^{j(\Omega t + \psi(\Omega, \omega))} \quad (8)$$

where the amplitude $E(\Omega, \omega)$ and $\psi(\Omega, \omega)$ can be written as

$$\left.\begin{aligned} E(\Omega, \omega) &= |R(\omega)| \,.\, |R(\omega + \Omega)| \\ \psi(\Omega, \omega) &= \phi(\omega + \Omega) - \phi(\omega) \end{aligned}\right\} \quad (9)$$

There are no theoretical limitations of RF frequency found in case of SSB modulation compared with DSB modulation to be opted in this work. This is due to only single-phase term associated with SSB modulation technique (Fig. 1).

2.2 Experimental setup for time-delay measurement of CFBG

Lightwave from the tunable laser source (*Yenista Optics: Model No. 1560/P6*) is provided to the optical input terminal of dual-drive MZM, whereas the other two input terminals of the MZM are fed with RF signal and DC biasing, as shown in Fig. 2. The amplified SSB modulated optical wave from erbium-doped fibre amplifier (EDFA) (*Thorlab EDFA 100S*) is reflected at a particular distance from the chirped grating depending on the wavelength corresponding to the Bragg condition. The reflected light is then divided into two arms by a 1×2 optical splitter, one arm is terminated by an OSA, whereas the second arm signal is sent to the digital spectrum oscilloscope (DSO) after passing through a 20 GHz bandwidth PD (*Optilab PD-20-M*). The time delay introduced in the microwave signal is determined by comparing the delayed microwave signal with the non-delayed microwave signal received directly from the RF signal generator.

2.3 Design and fabrication details of single-element rectangular patch antenna

A rectangular microstrip antenna (Fig. 3) has been designed, simulated, and fabricated at Ku band. The operating frequency is 13 GHz. Then, 1×8 microstrip antenna array is designed using single patch antenna. Each element of the array antenna is individually excited using coaxial feeding technique as shown in Fig. 4. Microstrip antenna consists of a thin metallic rectangular patch photoetched on the top side of the substrate (dielectric) having a fully conducting metallic ground plane below it. Flame retardant 4 (FR4) with dielectric constant $\varepsilon_r = 4.4$, loss tangent ($\tan\delta$) equal to 0.02, and thickness of 1.6 mm is used as substrate. This antenna is simulated in high-frequency structure simulator 3D electromagnetic computation tool and the necessary characteristics

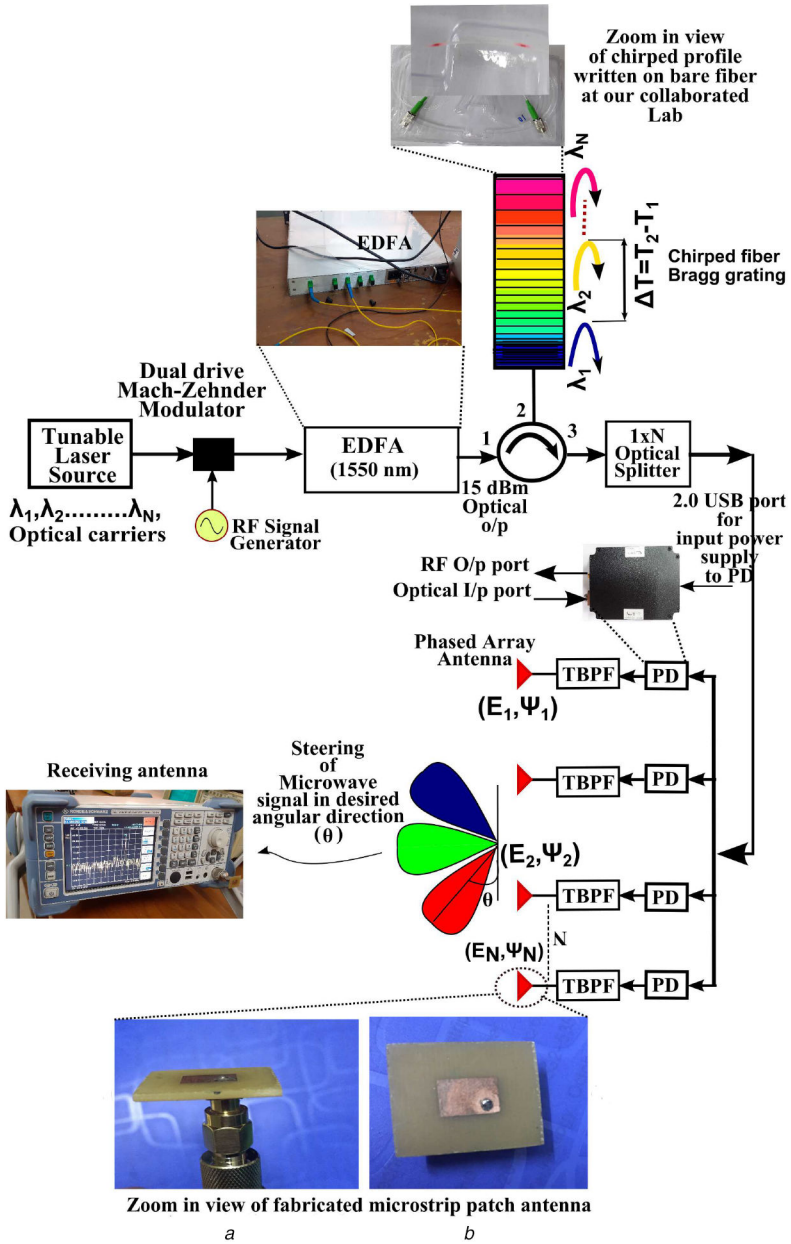

Fig. 1 *Proposed experimental setup for the beam-steering system (PD: photodetector, TBPF: tunable bandpass filter)*
(a) Patch antenna fed with photonically delayed microwave signal, ***(b)*** Top view of the fabricated patch antenna

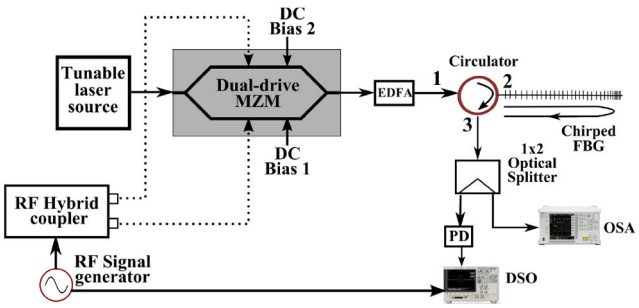

Fig. 2 *Schematic diagram of the experimental setup for measurement of time delay introduced by CFBG (MZM: Mach–Zehnder modulator, PD: Photodetector, DSO: Digital spectrum oscilloscope, EDFA: Erbium-doped fibre amplifier)*

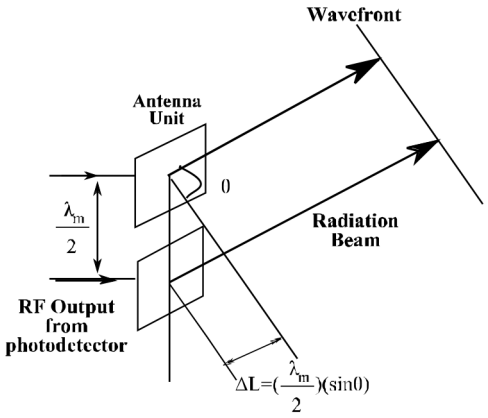

Fig. 3 *Single-PAA unit, radiation of beam, and its wavefront*

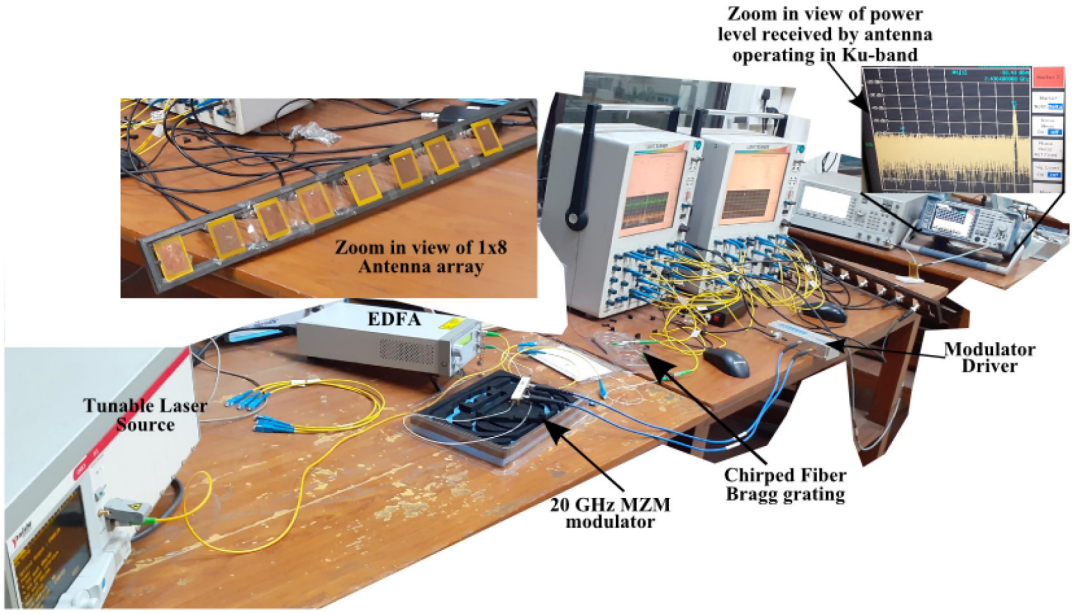

Fig. 4 *Proposed experimental setup for photonic feeding of 1 × 8 PAA (inset figure shows the 1 × 8 antenna array used and its resonant peak at 13 GHz)*

are mentioned in terms of return loss, voltage standing wave ratio, peak gain, and radiation patterns. The performance of the microstrip antenna depends on its dimension, the operating frequency, radiation efficiency, directivity, return loss, and other related parameters. For an efficient radiation, following equations are used for calculations. Practical width of patch is calculated using equation below [25]:

$$W = \frac{1}{2f_r\sqrt{\varepsilon_0\mu_0}}\sqrt{\frac{2}{\varepsilon_r+1}} \tag{10}$$

The effective dielectric constant ε_{eff} is given below:

$$\varepsilon_{\text{eff}} = \frac{\varepsilon_r+1}{2} + \frac{\varepsilon_r-1}{2}\left[1+\frac{12h}{w}\right]^{-(1/2)} \tag{11}$$

where ε_r is the dielectric constant of material, w is the width of patch, and h is the height of substrate. Prolonged electrical length ΔL of the patch due to fringing effect can be calculated using [25]

$$\Delta L = \frac{0.412(\varepsilon_{\text{reff}}+0.3)((w/h)+0.264)h}{(\varepsilon_{\text{reff}}-0.258)((w/h)+0.8)} \tag{12}$$

The effective length L_{eff} is given by

$$L_{\text{eff}} = \frac{v_0}{2f_r\sqrt{\varepsilon_{\text{eff}}}} - 2\Delta L \tag{13}$$

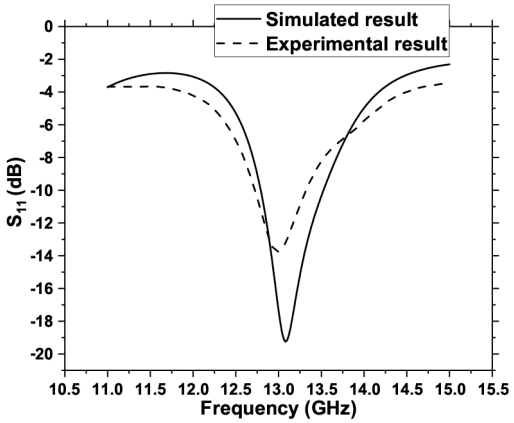

Fig. 5 *S_{11} (dB) versus frequency plot: simulated and experimental result of 1 × 8 array antenna*

Table 3 Dimension of fabricated 1 × 8 antenna array

Design parameters	Value
Operating frequency	13 GHz
Dielectric constant	4.4
Substrate thickness	1.6 mm
Substrate width	19 mm
Substrate length	23 mm
Patch length	9.3 mm
Patch width	6.2 mm
Radius of coax pin	0.2 mm

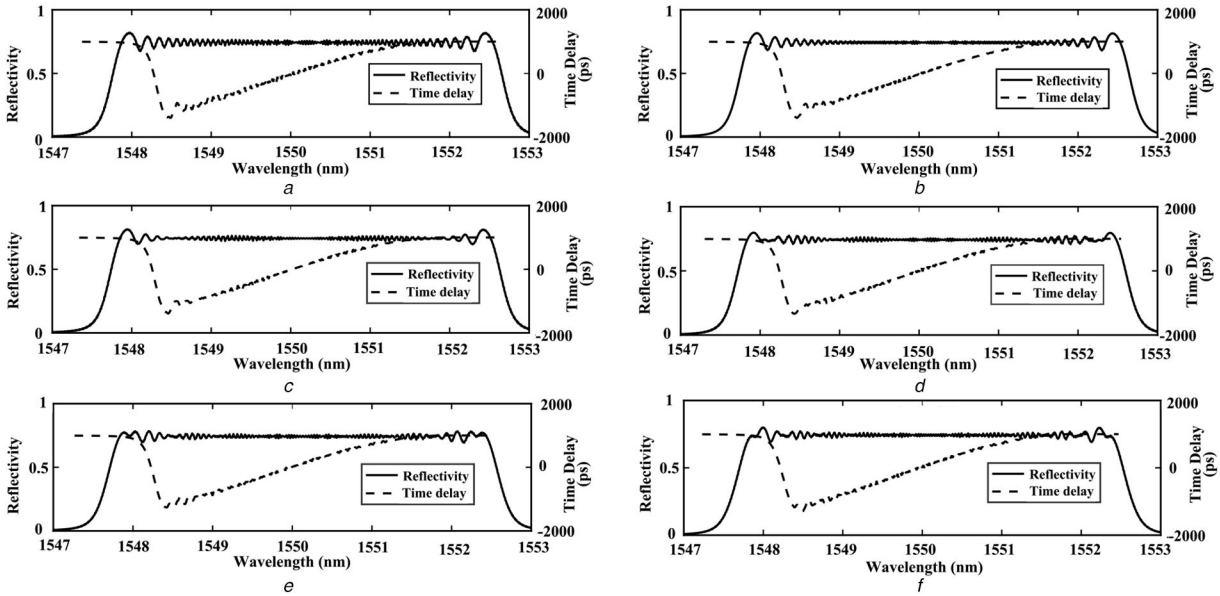

Fig. 6 *Grating reflectivity and time-delay responses while the light is modulated by SSB modulation technique at different RF frequencies*
(a) *Ω = 0 GHz,* ***(b)*** *Ω = 3 GHz,* ***(c)*** *Ω = 6 GHz,* ***(d)*** *Ω = 13 GHz,* ***(e)*** *Ω = 18 GHz,* ***(f)*** *Ω = 24 GHz*

The fabricated prototype of the proposed 1 × 8 phased array antenna is tested under vector network analyser for the S-parameter measurement practically. The simulated and experimentally obtained return loss characteristics have been presented in Fig. 5 that shows a good agreement with each other. According to observation, the experimental reading shows return loss is −13.8 dB at 13.0 GHz, whereas simulated results is −19.1 dB at 13.05 GHz. Detailed description of antenna parameters are given in Table 3. After electrical characterisation of a single antenna element, the array is formed on a wooden frame with equal spacing between successive elements, as shown in Fig. 4. After design, fabrication, and characterisation of antenna array, the TTD line is realised by using CFBG, which is discussed in the next section.

2.4 Design and fabrication of FBG for beam-steering applications

The detailed discussion on the FBG design and fabrication problem for the proposed experimental work is discussed in this section. It is a matter of fact that chirp rate should be high enough to be enabled to operate at high microwave frequency signal. Moreover, there is a limit on the chirp rate, which can be increased depending on the fabrication process and limitations associated with it. Fig. 6 shows that, in the case of single chirp grating, the time-delay response of the CFBGs is almost linear and independent of microwave frequencies. It is also apparent that the components of high microwave frequency deviate significantly more than the low microwave frequency. It is interesting to note that group delay of 3 GHz microwave signal crosses group delay of minimum microwave signal frequency at 1549.5 nm, as shown in Fig. 7.

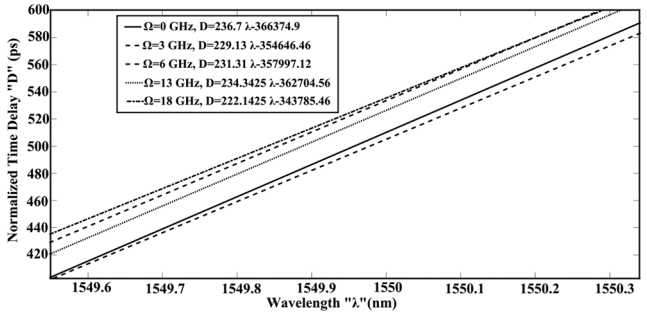

Fig. 7 *Experimentally measured time delays versus optical wavelength for the Linearly chirped fibre Bragg grating (LCFBG) TTD unit operating at various microwave frequencies*

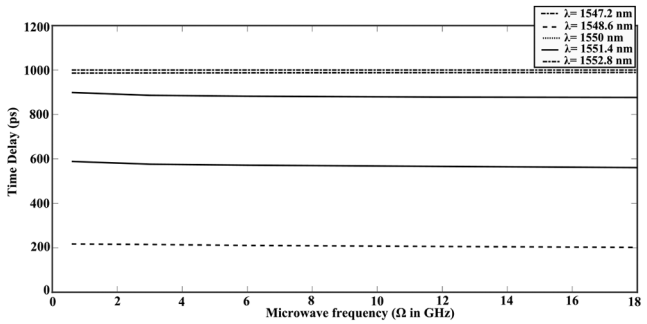

Fig. 8 *Measured time delays (ps) versus microwave frequencies for the LCFBG operating at various optical wavelengths*

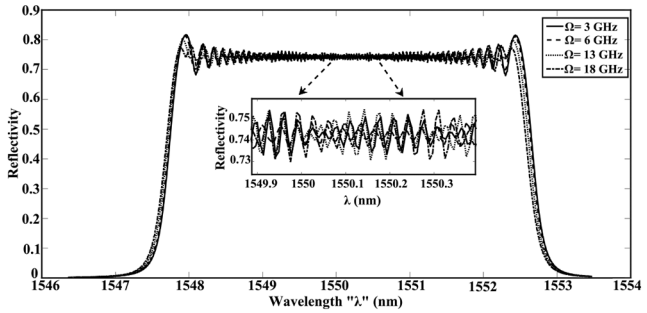

Fig. 9 *Grating reflectivity response as a function of optical wavelength at different modulation frequencies, namely* $\Omega = 3, 6, 13, 18$ GHz

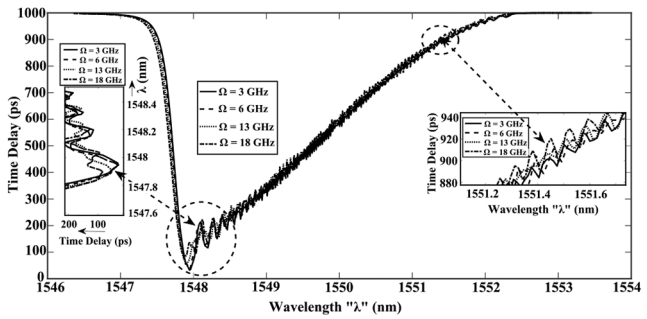

Fig. 10 *Group delay response as a function of optical wavelength at different modulation frequencies, namely* $\Omega = 3, 6, 13, 18$ GHz *(figure in the inset shows the zoom of the small section of the plot)*

Nevertheless, this function disappears with a 6 GHz microwave signal. At a higher microwave frequency such as 13 GHz, the group delay graph tends to become more linear. Linearity is more pronounced at $\lambda \geq 1549.8$ nm wavelength. Interesting feature comes at $\Omega = 13$ GHz, where there is a small variance of linearity relative to $\Omega = 6$ GHz. Also, the group delay response curve at $\Omega = 13$ GHz shows some marginal deviation in the range of $\lambda \leq 1550$ nm. However, for $\lambda \geq 1551$ nm, both curves are almost coincidental. Again, the observation is same at $\Omega = 18$ GHz. There is a marginal deviation with other lower microwave frequency components for $\lambda \leq 1548.8$ nm. The following observation shows that the group delay of CFBG is almost independent of the microwave frequency. Hence, CFBG is a TTD beam former and is very much suitable for wideband applications. It is also noted that the time delay of the microwave modulating signal can be substantially changed by scanning in optical frequency; the fact is reflecting in Fig. 8. Fig. 9 shows that the ripple in the reflectivity spectrum continues to decrease at a higher microwave frequency. One interesting feature is that at $\Omega = 13$ GHz ripples occur significantly in the central spectrum area but significantly reduced at the corner frequency of the spectrum. It is worth mentioning that the time delay of the modulated signal is independent of the RF frequency, and therefore the frequency of the modulating signal must be low enough to preserve the linewidth of the optical spectrum. It is evident from the time-delay response behaviour as shown in the inset of Fig. 10 that as the microwave frequency increases, the ripple decreases at the lower wavelength region $\lambda \leq 1550$ nm, while this behaviour reverses for the region away from the centre wavelength $\lambda \geq 1550$ nm.

To validate the theoretical results, a CFBG with central Bragg wavelength $\lambda_B = 1550$ nm and 1.55 nm bandwidth with reflectivity 90.95% has been fabricated. The experimentally obtained wavelength span of maximum reflectivity bandwidth comes to be ≃1548–1553 nm. The fabricated grating (as shown in Fig. 1) has a length of ≃ 5 cm and chirp factor $D\lambda_D \simeq 0.5e^{-6}$ nm/cm. The phase of chirp has been calculated by the following expression:

$$\frac{1}{2}\frac{d\phi}{dz} = -4\pi\frac{n_{eff}}{z}D\lambda_D\lambda_B^2 \tag{14}$$

where $n_{eff} \simeq 1.45$, z is the length of grating, and λ_B is the Bragg wavelength. The far-field radiation pattern of N-element phased array antenna with the spacing between each element d is given by

$$AF(\theta) = \sum_{i=0}^{N-1} E_i(\Omega, \omega_i)e^{j\left(\psi_i(\Omega, \omega_i) + i\left(\frac{\Omega d \sin\theta}{c}\right)\right)} \tag{15}$$

The beam-pointing angle corresponding to the main lobe of the array antenna can be expressed in terms of the grating time delay as follows:

$$\sin\theta_0 = \frac{c}{d}[\tau(\omega_i) - \tau(\omega_{i-1})] \tag{16}$$

This ensures that the beam-pointing direction depends on the spacing of two consecutive time delays introduced by the grating and is independent of the microwave frequency. It is worth mentioning that the beam angle can be modified by changing the time-delay response of the grating. It should be noted that the minimum steering angle step size θ_{min} can be expressed as

$$\frac{1}{2f_m}\sin(\theta_{min}) = |\Delta\tau|_{min} \tag{17}$$

where $|\Delta\tau|_{min}$ is the minimum acceptable time delay between adjacent points of reflection from single chirp grating. It also means that minimum steerable angle depends on modulating microwave signal. If a single chirp grating works as a delay line as shown in Fig. 3, the time delay between adjacent points of the reflections can be written as

$$|\Delta\tau|_{min} = \frac{2nd_{min}}{c} \tag{18}$$

where d_{min} is the minimum distance of two adjacent reflections of CFBG, f_m is the modulating signal frequency, and n is the refractive index of optical fibre. From (17) and (18), we can interpret that the minimum steerable angle step size θ_{min} can be expressed as

$$\theta_{\min} = \sin^{-1}\left(\frac{4nf_m d_{\min}}{c}\right) \tag{19}$$

3 Experimental result

3.1 Observation sheet for various parameters at $\Omega = 3$ GHz *microwave frequency*

Table 4 shows the observation sheet of measured theoretical and experimental values of reflected light intensity through fabricated featured chirp FBG along with their measured phases. Fig. 3 shows the proposed experimental setup for the measurement of time delay, phase, and reflection spectrum of chirp FBG. Theoretically, phase has been calculated at different wavelengths by calculating angle of reflection amplitude from chirp FBG. The phase of RF signal is calculated theoretically by linear approximation of group delay plot followed by the expression:

$$\psi(\Omega, \omega) = -\tau(\omega) \,.\, \Omega$$

where parameter $\tau(\omega)$ has been estimated by actual simulation plot and their linear approximation plot of group delay response as described in Fig. 11.

Since the total grating length is 50 mm; hence, for the present case, i.e. for $\Omega = 3$ GHz, the maximum spacing between grating should be 99.97 mm (that is maximum grating spacing irrespective of initial point). As a result of this, all the frequency components will participate in beam-steering process. Since the minimum time delay offer for present case is 36.7 ps corresponding to $d_{\min} = 3.67$ mm, we can calculate the minimum steering angle step size

$$\theta_{\min} = \sin^{-1}\left(\frac{4nf_m d_{\min}}{c}\right) \simeq 12.6^{\circ}$$

To increase the resolution and discrimination factor, the CFBG has to be designed with proper specifications to achieve the minimum steer angle step size $\theta_{\min}$. Now, for the present case, it has been assumed that the time delay is almost linear approximation of grating length. However, this linear approximation does not completely follow the actual chirped grating response due to the presence of ripple in the time-delay response of the grating. Fig. 11 shows the actual computed group delay response for the proposed design of chirp FBG at $\Omega = 3$ GHz. The dispersion slope ($D\lambda$) obtained by linear approximation is ~225.25 ps/nm. Fig. 11 also shows the obtained group delay response of CFBG followed by linear approximation. It is apparent that ripples are more intensified at lower wavelength region; hence, some error is introduced in calculation of maximum steerable angle.

There is a small error introduced in beam radiation pattern due to imperfection of initial and corner values of time-delay response and magnitude. Fig. 12*a* shows the theoretically calculated array factor (AF) at various wavelengths as mentioned in the caption of this figure. Fig. 12*b* shows the corresponding radiation pattern for 8-element array. Figs. 13*a–e* shows the radiation pattern for variable elements of PAA at $\Omega = 3$ GHz. It is apparent that theoretical results have a good resemblance with experimental one. In some cases, both experimental and theoretical results are overlapped and could not be discriminated in these plots. Tables 4 and 5 have been followed to obtain Fig. 13. Fig. 13*f* shows the actual group delay and its linear approximation plot at $\Omega = 3$ GHz. The dispersion slope ($D\lambda$) is directly related with chirp rate of fabricated FBG. It is evident that the dispersion slope ($D\lambda$) keeps on tailored with the modulating microwave frequency Ω.

Fig. 14 shows the theoretically computed group delay response and its corresponding first-order linear approximation at $\Omega = 6$ GHz. It is apparent that the dispersion slope is reduced for this case as compared with $\Omega = 3$ GHz. It is a matter of fact that reduction of dispersion slope would eventually increase the effective grating linear length; hence, there is trade-off between both the quantities. Evidently, increasing of effective length of linear region would enhance the maximum range of steerable angle squint free.

Fig. 15 shows the radiation pattern for variable elements of PAA at $\Omega = 6$ GHz. It is apparent that compared with $\Omega = 3$ GHz, the maximum angle which can be steered for $N = 16$ number of elements would be $\theta = \pm 73^{\circ}$. Fig. 15*f* shows the corresponding time-delay response and its first-order linear approximation. Figs. 16 and 17 shows the similar results at microwave frequency $\Omega = 13$ GHz. It means that as the modulating microwave frequency Ω increases, dispersion slope reduced, which will, in turn, effectively increase the grating spacing followed by grating length, because of increase of maximum beam-steerable angle. Experimental results have a good agreement with the theoretical results. It also appears that side lobes in a radiation pattern can be

Table 4 Observation at $\Omega = 3$ GHz microwave frequency

Sl. no.	Wavelength (λ), nm	Theoretical $E_i(\Omega, \omega_i)$	Experimental $E_i(\Omega, \omega_i)$	Theoretical $\psi_i(\Omega, \omega_i)$, rad	Experimental $\psi_i(\Omega, \omega_i)$, rad
1	1548	0.7206	0.692	−3.8	−2.9
2	1548.5	0.9542	0.922	1.25	1.01
3	1549	0.9537	0.956	−0.072	0.32
4	1549.5	0.9331	0.892	−1.355	−2.11
5	1550	0.980	0.973	−2.637	−1.82
6	1550.5	0.9701	0.957	−3.990	−2.19
7	1551	0.9851	0.974	0.9929	1.3
8	1551.5	0.9731	0.643	0.0607	0.31
9	1552	0.9137	0.923	−0.1455	−0.31
10	1552.5	0.7979	0.773	−0.24	−0.31

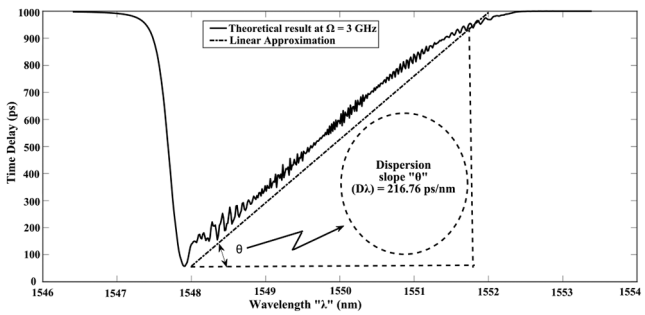

Fig. 11 *Theoretical group delay response and their linear approximation versus optical wavelength at* $\Omega = 3$ GHz

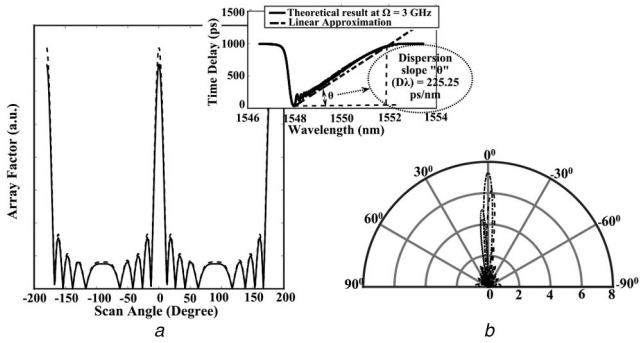

Fig. 12 *Theoretically calculated AF at various wavelengths*

(a) Estimated AF and their beam-steering capability for various wavelengths at $\Omega = 3$ GHz [inset figure shows the corresponding time-delay response], ***(b)*** Radiation pattern ($\theta = 0°$) of beam corresponding to dispersion slope $D\lambda = 225.25$ ps/nm for 8-element antenna array

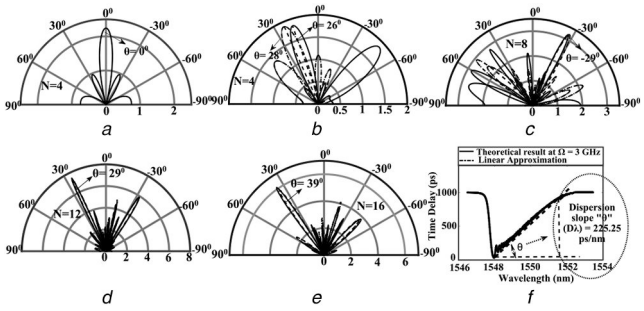

Fig. 13 *Radiation pattern of*

(a), (b) 4, ***(c)*** 8, ***(d)*** 12, ***(e)*** 16 elements of PAA steered by the proposed TTD unit at $\Omega = 3$GHz. Inset figure ***(f)*** shows the corresponding group time-delay response and its first-order linear approximation

Table 5 Theoretically and experimentally measured time delay versus wavelength at $\Omega = 3$ GHz microwave frequency

Sl. no.	Wavelength, nm	Theoretical time delay by linear approximation, ps	Actual time delay by computation, ps	Experimental time delay, ps	Grating spacing computation, mm	Grating spacing experimental, mm
1	1548	36.7	36.5	36.43	3.65	3.64
2	1548.5	84.14	118.5	123.3	11.85	12.33
3	1549	178.7	203.8	197.8	20.38	19.78
4	1549.5	382.21	408.4	403.5	40.84	40.35
5	1550	604.7	628.8	613.5	62.88	61.35
6	1550.5	612.3	703.5	711.1	70.35	71.11
7	1551	628.5	841.62	823.3	84.16	82.33
8	1551.5	811.4	983.5	986.5	98.35	98.65
9	1552	983.5	988.8	973.4	98.88	97.34
10	1552.5	N.A.	988.8	982.4	98.88	98.24
11	1553	N.A.	999.7	995.6	99.97	99.56

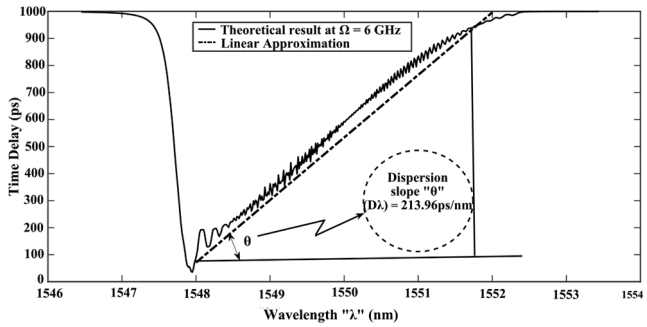

Fig. 14 *Calculated group delay (ps) vs optical wavelength response at* $\Omega = 6$ GHz

tailored by controlling chirp rate of chirp FBG, which is again an area of great attention as an outcome of this research paper. Fig. 17 shows the theoretically computed group delay (ps) response and its corresponding first-order linear approximation at $\Omega = 13$ GHz. It is to be noted that the dispersion slope does not significantly change compared with the previous case. It is also evident that ripples are reduced at lower wavelength region compared with previous cases. Figs. 16*a–e* show the radiation pattern for variable number of antenna elements at $\Omega = 13$ GHz. It is to be noted that the steering angle has main lobes at different directions as number of antenna element increase. In some cases, theoretical results are overlapped with the experimental results not distinguishable. However, in

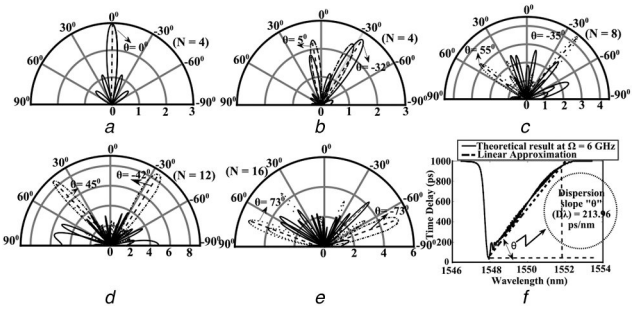

Fig. 15 *Radiation pattern of*
(a), (b) 4, ***(c)*** 8, ***(d)*** 12, ***(e)*** 16 elements of PAA steered by the proposed TTD unit at Ω = 6 GHz. Inset figure ***(f)*** shows the corresponding group time-delay response and its first-order linear approximation

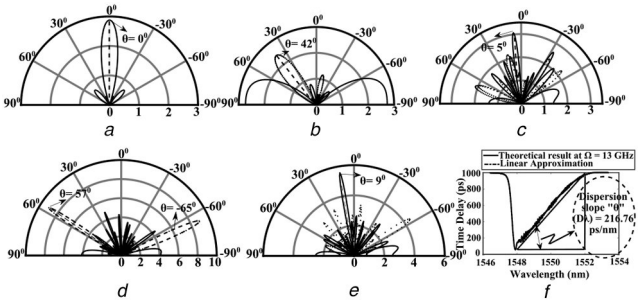

Fig. 16 *Radiation pattern of*
(a), (b) 4, ***(c)*** 8, ***(d)*** 12, ***(e)*** 16 elements of PAA steered by the proposed TTD unit at Ω = 13 GHz. Inset figure ***(f)*** shows the corresponding group time-delay response and its first-order linear approximation

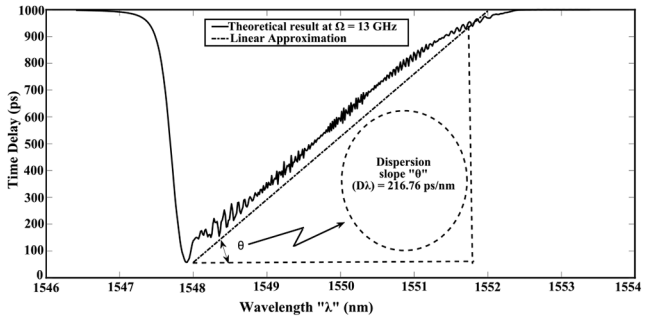

Fig. 17 *Theoretical group delay (ps) vs optical wavelength response at* Ω = 13 GHz

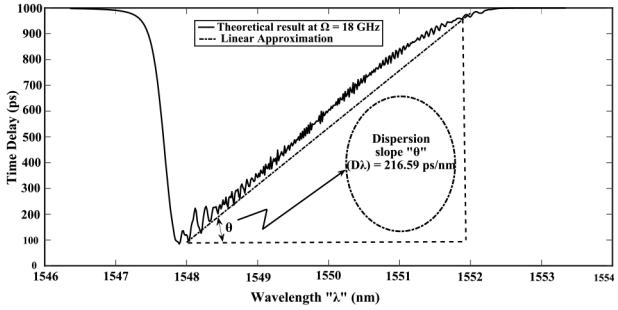

Fig. 18 *Graph of group delay (ps) vs optical wavelength response of proposed system at* Ω = 18 GHz

some cases, they are distinguishable. Inset Fig. 16*f* shows the corresponding group delay response and its first-order linear approximation.

Fig. 18 shows the theoretically computed group delay (ps) response and its corresponding first-order linear approximation at Ω = 18 GHz. For this case, dispersion slope does not vary compared with Ω = 13 GHz as shown in Fig. 16. Figs. 19*a–e* show the radiation pattern for variable number of antenna elements at Ω = 18 GHz. It is evident that beam-steering angle significantly pointed out toward large angle compared with the previous case. In this case, theoretical results have good correlation factor with

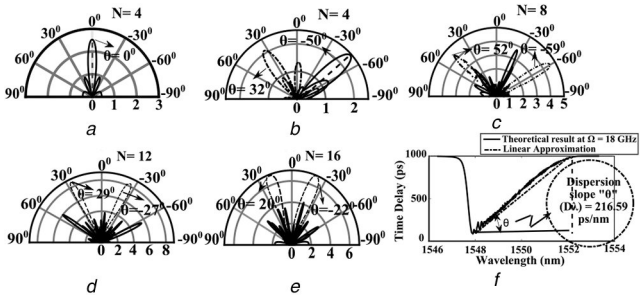

Fig. 19 *Radiation pattern of*
(a), (b) 4, ***(c)*** 8, ***(d)*** 12, ***(e)*** 16 elements of PAA steered by the proposed TTD unit at Ω = 18 GHz (Ku band). Inset figure ***(f)*** shows the corresponding group time-delay response and its first-order linear approximation

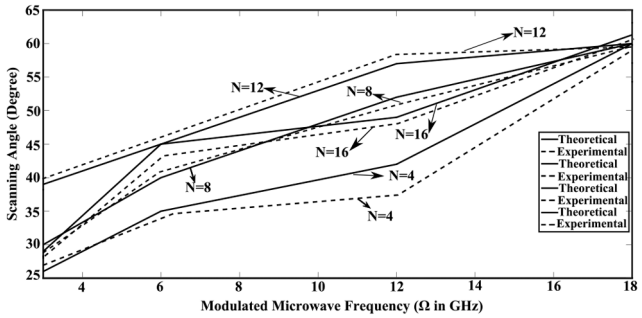

Fig. 20 *Scanning angle versus modulating microwave frequency and number of antenna elements*

experimental results. Fig. 20 shows the variation of scanning angle with modulating microwave frequency for a variable number of antenna array elements. It is observed that scanning angle increases, in general, as the number of antenna element and microwave frequency increases. Scanning angle has maximum value for particular value of modulating frequency for each case. There is a slight variation of theoretical results with the experimental one due to imperfection in the measurement process.

Table 6 Comparison between TTD modules: CFBG and discrete FBG

Sl. no.	FBG scheme	Beam-steering angle, deg	Sidelobe levels, dB	Scanning loss	Insertion loss, dB
1	CFBG	±75	−20	low	<1
2	Discrete FBG	±40	−2	moderate	≃3.2

4 Conclusion

To the best of our knowledge, the beam-steering capability offered by special featured CFBG has not been explored by any researcher till date. Table 6 shows the benefits of using CFBG as a TTD module when compared discrete or uniform FBG-based TTD module for beam steering. Since the dispersion slope is directly related to the chirp rate of the CFBG, a detailed investigation of the dispersion slope characteristics of the CFBG has been presented by taking care of this point. Chirp FBG has been fabricated with the desired specification at collaborated laboratory. Beam-steering capabilities have been explored for the chirp parameter and the dispersion slope at the microwave frequency range from the S band to Ku band. Array antenna has been fabricated working up to Ku band. Theoretical results have been validated with experimental results. The maximum beam-steering angle for microwave frequency and number of antenna elements have been further exploded validating with found results in the literature.

5 Acknowledgments

Authors express their deepest appreciation and gratitude to Mr. R.K. Bhal, Head of the Optical Communications Division, Satellite and Navigation payload area, Space Application Centre (SAC)-Indian Space Research Organisation (ISRO), Ahmedabad, India for financially supporting this work under the ISRO Respond project (Project no.: ISRO/(10)/2018-2019/571/ECE and Grant no.: DS-2B-13012(2)/13/2018) entitled as 'A novel Mach–Zehnder modulator based integrated photonic highly steerable beamforming system for broadband satellite communication link'. Authors also thank Dr. Om Prakash, Shri S.V. Nakhe, Director, Laser Group RRCAT; Dr. S.K. Dixit, Head of the Fibre Sensors and Optical Spectroscopy Section (FSOSS), Raja Ramanna Centre for Advanced Technology, Indore for fabricating CFBG with the desired specifications.

6 References

[1] Pisco, M., Spirito, M., Cutolo, A., *et al.*: 'Improved photonic true time delay unit for a Ku-band phased array antenna demonstration', *Open Opt. J.*, 2008, **2**, pp. 35–40

[2] Zhou, B., Zheng, X., Yu, X., *et al.*: 'Impact of group delay ripples of chirped fiber grating on optical beamforming networks', *Opt. Express*, 2008, **16**, (4), pp. 2398–2404

[3] Verpoorte, J., Schippers, H., Jorna, P., *et al.*: 'Architectures for Ku-band broadband airborne satellite communication antennas', National Aerospace Laboratory NLR, 2010

[4] Tessema, N.M.: 'Optical control of radio beam steering for broadband satellite communication', Technische Universiteit Eindhoven, 2017

[5] Iupikov, O.A., Ivashina, M.V., Skou, N., *et al.*: 'Multibeam focal plane arrays with digital beamforming for high precision space-borne ocean remote sensing', *IEEE Trans. Antennas Propag.*, 2018, **66**, (2), pp. 737–748

[6] Jiang, Y., Howley, B., Shi, Z., *et al.*: 'Dispersion-enhanced photonic crystal fiber array for a true time-delay structured x-band phased array antenna', *IEEE Photonics Technol. Lett.*, 2005, **17**, (1), pp. 187–189

[7] Srivastava, N.K., Raghuwanshi, S.K.: 'Demonstration of highly steerable beamforming system incorporating a waveguide of spatially distributed fiber Bragg grating'. 2019 Sixth Int. Conf. Signal Processing and Integrated Networks (SPIN), Noida, India, 2019, pp. 367–370

[8] Srivastava, N.K., Srivastava, A., Raghuwanshi, S.K.: 'Microwave waveform generation with high chirp rate and central frequency using dual-parallel Mach–Zehnder modulator for an efficient microwave beam steering network', *Microw. Rev.*, 2018, **24**, (2), pp. 3–8

[9] Pisco, M., Campopiano, S., Cutolo, A., *et al.*: 'Continuously variable optical delay line based on a chirped fiber Bragg grating', *IEEE Photonics Technol. Lett.*, 2006, **18**, (24), pp. 2551–2553

[10] Tosi, D.: 'Review of chirped fiber Bragg grating (CFBG) fiber-optic sensors and their applications', *Sensors*, 2018, **18**, (7), p. 2147

[11] Molony, A., Zhang, L., Williams, J.A., *et al.*: 'Fiber Bragg-grating true time-delay systems: discrete-grating array 3-b delay lines and chirped-grating 6-b delay lines', *IEEE Trans. Microw. Theory Tech.*, 1997, **45**, (8), pp. 1527–1530

[12] Mousavi, P., Fakharzadeh, M., Jamali, S.H., *et al.*: 'A low-cost ultra-low profile phased array system for mobile satellite reception using zero-knowledge beamforming algorithm', *IEEE Trans. Antennas Propag.*, 2008, **56**, (12), pp. 3667–3679

[13] Yegnanarayanan, S., Jalali, B.: 'Wavelength-selective true time delay for optical control of phased-array antenna', *IEEE Photonics Technol. Lett.*, 2000, **12**, (8), pp. 1049–1051

[14] Howley, B., Wang, X., Chen, M., *et al.*: 'Reconfigurable delay time polymer planar lightwave circuit for an x-band phased-array antenna demonstration', *J. Lightwave Technol.*, 2007, **25**, (3), pp. 883–890

[15] Shi, S., Bai, J., Schneider, G.J., *et al.*: 'Conformal wideband optically addressed transmitting phased array with photonic receiver', *J. Lightwave Technol.*, 2014, **32**, (20), pp. 3468–3477

[16] Shi, Z., Gu, L., Howley, B., *et al.*: 'True-time-delay modules based on a single tunable laser in conjunction with a waveguide hologram for phased array antenna application', *Opt. Eng.*, 2005, **44**, (8), p. 084301

[17] Weiss, S., Keller, S., Ly, C.: 'Development of simple affordable beamformers for army platforms'. Proc. GOMACTech–07 Conf., Lake Buena Vista, FL, 2006

[18] Rahimian, A.: 'Design and performance of a [k. Sub. u]-band Rotman lens beamforming network for satellite systems', *Prog. Electromagn. Res. M*, 2013, **28**, pp. 41–56

[19] Liu, Y., Yang, J., Yao, J.: 'Continuous true-time-delay beamforming for phased array antenna using a tunable chirped fiber grating delay line', *IEEE Photonics Technol. Lett.*, 2002, **14**, (8), pp. 1172–1174

[20] Chen, D., Xiang, P., Wang, R., *et al.*: 'Beamforming system based on paralleled variable chirped microwave signal generators', *J. Opt. Technol.*, 2017, **84**, (6), pp. 390–394

[21] Schippers, H., Verpoorte, J., Jorna, P., *et al.* 'Broadband optical beamforming for airborne phased array antenna'. 2009 IEEE Aerospace Conf., Big Sky, MT, USA, 2009, pp. 1–19

[22] Yang, J., Liu, Y., Tjin, S.C., *et al.*: 'Tunable chirped fiber grating based variable time-delay network for phased-array antenna beamforming', *Int. J. Infrared Millim. Waves*, 2003, **24**, (4), pp. 593–601

[23] Zhou, W., Stead, M., Weiss, S., *et al.*: 'Developing an integrated photonic system with a simple beamforming architecture for phased-array antennas', *Appl. Opt.*, 2017, **56**, (3), pp. B5–B13

[24] Li, M., Yao, J.: 'Photonic generation of continuously tunable chirped microwave waveforms based on a temporal interferometer incorporating an optically pumped linearly chirped fiber Bragg grating', *IEEE Trans. Microw. Theory Tech.*, 2011, **59**, (12), pp. 3531–3537

[25] Stutzman, W.L., Thiele, G.A.: '*Antenna theory and design*' (John Wiley & Sons, Inc., New York, USA, 2012)